1. Lichtmikroskopie

Axiophot Zeiss

Auflichtmikroskop Hellfeld, Dunkelfeld, Polarisation, Interferenzkontrast (DIK)

Objektive: x1,25; x2,5; x5; x10; x20; x50; x100

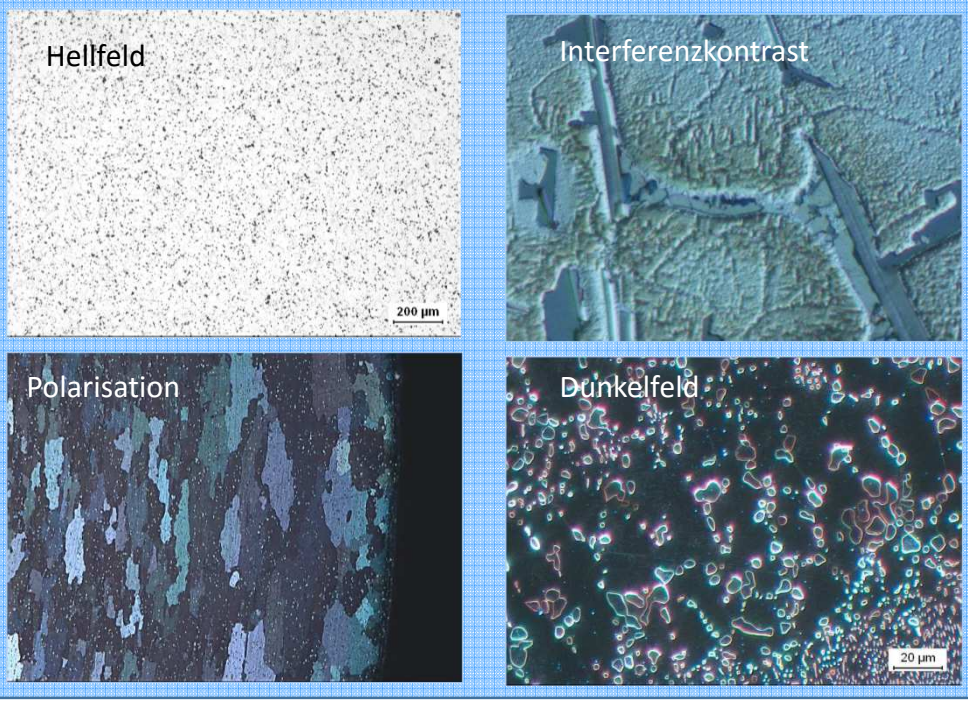

2. Laserscanningmikroskop

LEXT OLS4000

3D-Laser-Scanning-Mikroskop

- Rauheitsmessungen, *berührungslos Polarisation, DIF*
- *Auflösung: x-y = 0,12µm / z = 0,01µm*
- *Objektive: x5; x10; x20; x50*; x100; x100(LD)

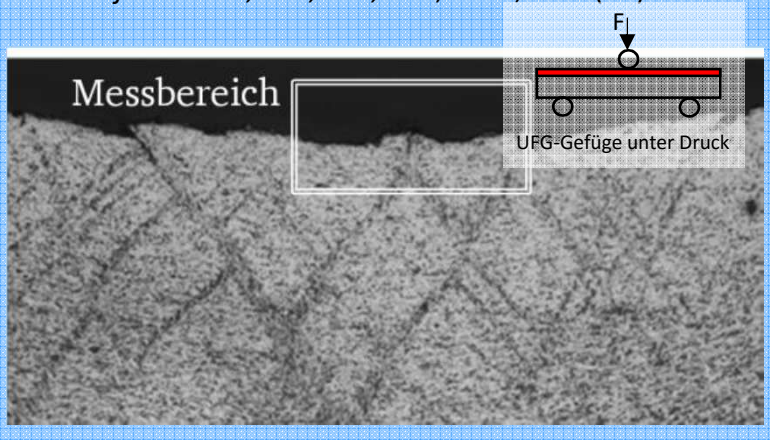

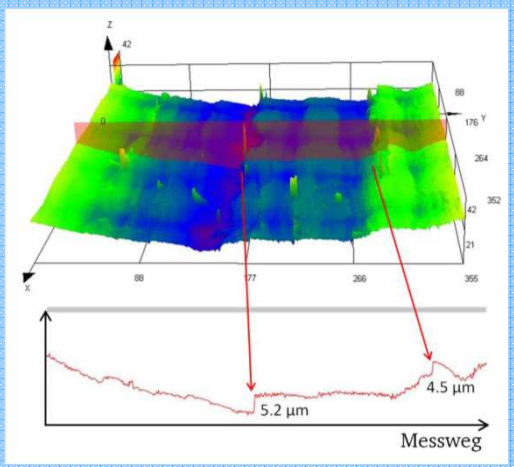

TECHNISCHE UNIVERSITÄT DARMSTADT

3. Rasterelektronenmikroskop

Tescan MIRA3-XM

- Installation: 2015
- Auflösung: 1nm
- Ausstattung: Schottky Field Emitter, wide field optics, 2 SE detectors (Everhart-Thornley, in-lens), BSE (high reolution, high temperature, low voltage imaging), Deben Gen5,

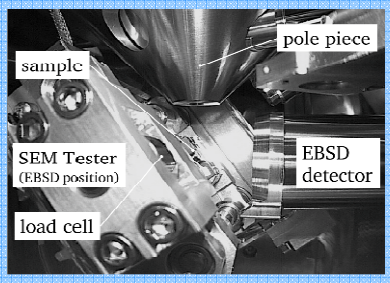

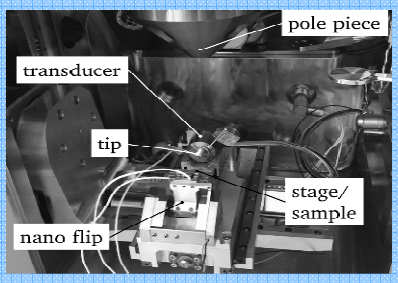

Electron channeling contrast imaging (ECCI)

The Tescan MIRA3 SEM is equipped with a four quadrant solid state BSE detector which facilitates the study of deformation microstructures via electron channeling contrast imaging (ECCI).

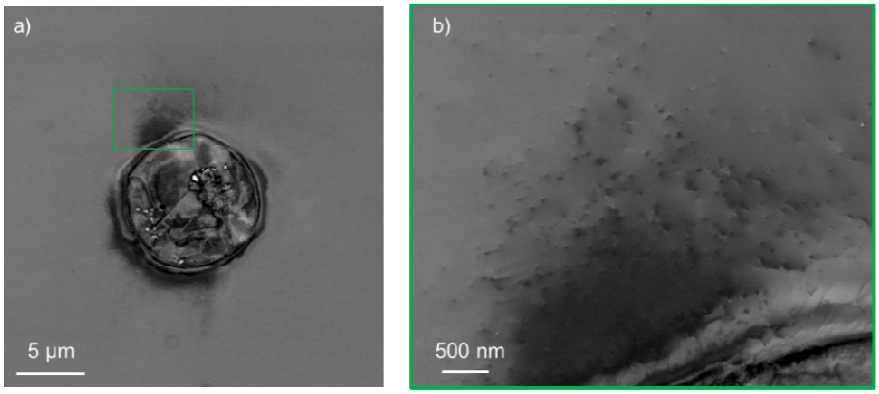

Fig. 1: ECCI images acquired around a ball indentation in Tungsten. The dark contrast in (b) stems from individual dislocations induced by the indentation.

The intensity of backscattered electron is strongly influenced by the orientation of crystal lattice planes with respect to the incident beam. A slight local misorientation in deformed regions can lead to different electron channeling conditions compared to non-deformed neighboring regions which enables the imaging of defects with enhanced contrast. Fig. 1(a) shows a ball nanoindentation image obtained via ECCI on coarse grained polycrystalline tungsten. Next to the residual impression, there is a significant contrast showing a deformed region with higher dislocation density which is marked by a rectangle. For better visualization, the highlighted region is shown in Fig. 1(b) which illustrates the dislocation structure around the ball nanoindentation. In future, the analysis of the local dislocation structure via ECCI will be used for a wide range of investigations such as dislocations at grain boundaries, crack tips or in highly deformed regions of the materials after indentation testing. This information is important for understanding the evolution of dislocation microstructures, which are essential for the thermomechanical properties of metallic materials.

EBSD analysis with high spatial and angular resolution

Electron Back Scatter Diffraction (EBSD) is used to analyze the local orientation or misorientation of individual grains based on corresponding electron diffraction patterns. The new SEM is equipped with an EDAX Octane Plus SDD EDX and a DigiView high resolution EBSD system which allows EBSD mappings with up to 200 frames per second on standard samples and 50-100 patterns per second on severely deformed ultrafine grained materials or when combining EDX and EBSD.

Grain size analysis

For nanocrystalline materials with a grain size below 100 nm, conventional EBSD reaches its resolution limits as the interaction volume of the electron beam in which the diffraction pattern is similar to or even larger than the grain size. However, EBSD can still be utilized to analyze nanocrystalline materials if a different measurement setup is being used. The size of the interaction volume can be reduced significantly when using thin electron transparent samples, such as those used for TEM investigations. The setup for a transmission EBSD measurement is shown in Fig. 2 together with the results on a severely deformed CuZn5 alloy with ultrafine grained microstructure.

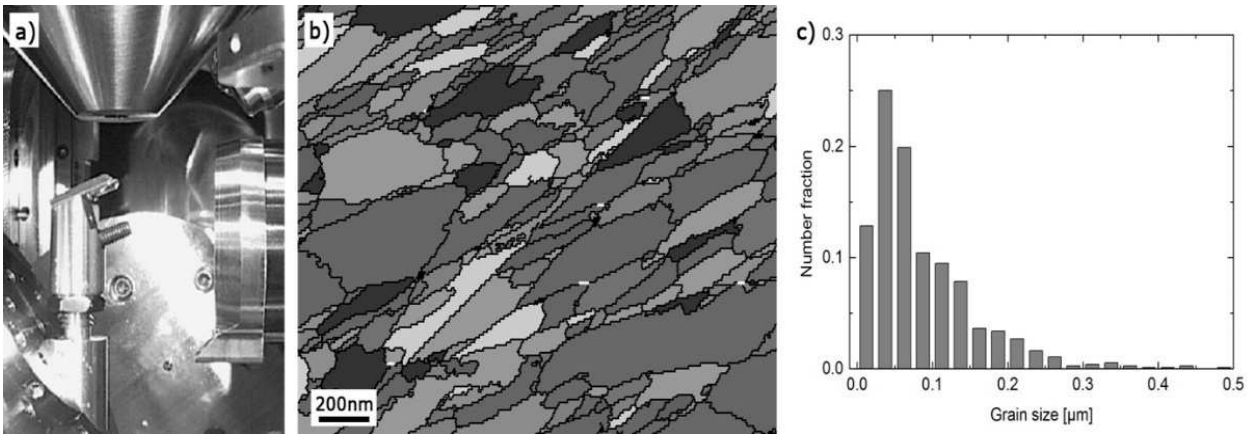

Fig. 2: Setup for transmission-EBSD (a) and grain map (b) with corresponding grain size distribution (c) of a t-EBSD measurement on UFG CuZn5.

While the micrograph appears to consist mostly of grains in the 300 – 500nm range, the grain size distribution clearly shows that the majority of grains are well below 100 nm, which could not be resolved in a standard EBSD setup. The analysis of the grain size distribution is of crucial for understanding the processes in the alloys, which enable the formation of an ultrafine grained microstructure during severe plastic deformation. Moreover, investigations on texture evolution or thermal stability of such alloys also require high resolution EBSD analysis.

Determination of dislocation density

EBSD can also be used for analyzing elastic and plastic strains inside the material. For these applications, the angular resolution of EBSD can be a limiting factor. The typical indexing approach with an angular resolution of 0.5 to 1° can't capture elastic strains and only allows a very rough estimate of the so called geometrically necessary dislocations (GNDs) if the dislocation density is sufficiently high. The angular resolution can be improved by about two orders of magnitude when using a different approach for misorientation measurements which is based on a digital image cross correlation of high resolution diffraction patterns. The same approach allows the determination of elastic strains with a resolution in the order of 10^{-4}.

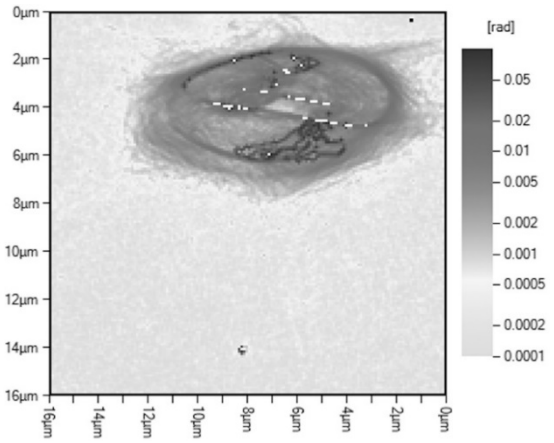

Fig. 3: High resolution Kernel Average Misorientation map of the plastic zone under a ball nanoindentation in Tungsten.

Hence the visualization of small plastic strain gradients and accurate quantification of GNDs becomes the cross correlation approach is demonstrated in Fig. 3 showing the plastic zone under a ball nanoindentation in Tungsten (same indent as in Fig. 1). The high resolution Kernel Average Misorientation (KAM) map illustrates the strain gradients within the plastic zone and evolving subgrain boundaries as dark lines with sharp contrast. The resolved KAM range covers more than two orders of magnitude from an orientation noise floor of approx. 0.01° (0.0002rad) up to 5° (0.1rad) at subgrain boundaries.

In-situ mechanical testing

Within the SEM chamber, an MTII/Fullam SEMtester universal testing machine (tension, compression, bending) can be installed for in-situ mechanical testing. Exchangeable load cells facilitate experiments in a load range from a few Newton up to 9 kN with crosshead velocities from < 1 µm/s to 80 µm/s. The device also features a heating unit which allows in-situ heat treatments and thermomechanical tests from RT up to >1000°C. Fig. 4 shows an example for an in-situ 3 point bending test in which the deformation behavior of ultrafine grained (UFG) steel is studied. High resolution BSE images show that the imposed bending displacements results in the formation and growth of shear bands while regions in between the shear bands remain strain free.

The formation of shear bands or other instabilities like necking in tensile testing or the propagation of cracks are strongly influenced by the material microstructure and loading condition. Here, in-situ high resolution analysis offers the unique possibility to correlate the instability with the local microstructure and deformation state.

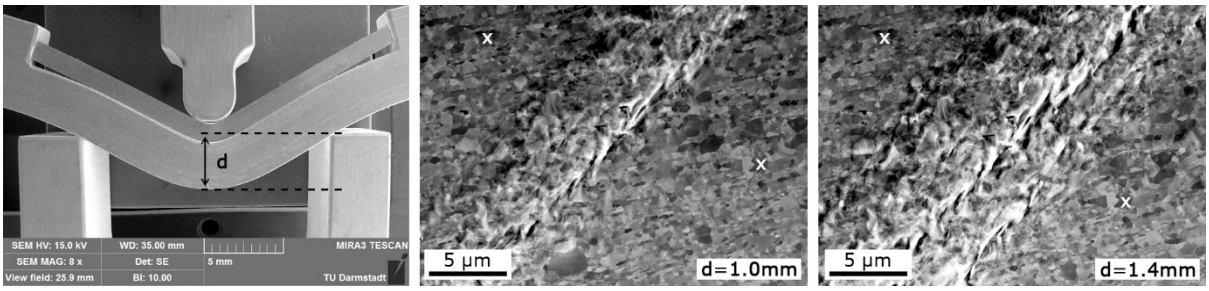

Fig. 4: Growth of a shear band in UFG steel during 3 point bending test (x markers indicate same positions).

In-situ Nanoindentation

Finally, the MIRA3 can be equipped with a new stage mounted cradle based in-situ nanoindenter called NanoFlip (Nanomechanics Inc., USA). The electromagnetic actuator of NanoFlip with a maximum force of 50 mN is capable to perform not only quasi-static but also dynamic testing in vacuum with frequencies of up to 500 Hz. The continuous measurement of contact stiffness or continuous dynamics analysis during dynamical testing allows for a detailed investigation of the mechanical behavior of a wide range of materials. Here the option of high speed data acquisition with up to 100 kHz provided by NanoFlip is beneficial for gaining a better understanding of the underlying deformation mechanisms.

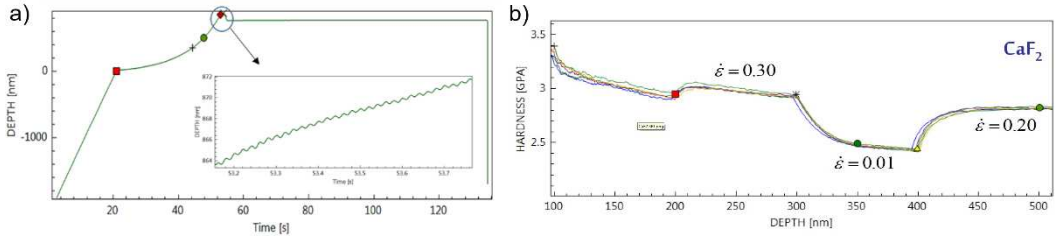

Fig. 5: a) Displacement resolution of actuator b) Hardness – Strain rate sensitivity on single crystalline CaF_2

The high performance of the indenter enables test methods such as strain-rate jump tests used to measure strain rate sensitivity on a very local scale. Figure 1 illustrates the displacement resolution and high speed data acquisition of the NanoFlip exemplarily shown for strain-rate jump test data measured on single crystal of CaF_2. Strain-rate variation leads to a significant change in hardness in single crystalline CaF_2 as shown in Fig. (b). These type of measurements can also be performed with the Nanomechanics and Keysight ex-situ nanoindenters which were recently installed in the PhM group. Mounting a sample in an SEM NanoFlip allows to automatically tilt the indenter stage by 90° to align the sample either in line with the SEM for high resolution imaging or the indenter tip for in-situ testing. The high resolution imaging and analytic capabilities of the SEM (EBSD and EDX) in combination with high positioning accuracy of the NanoFlip allow site specific testing of small volumes such as individual phases in a complex microstructure. This is exemplarily shown in Fig. 7 for Austempered Ductile Iron (ADI), which consists of several phases with different mechanical properties. Unlike martensite and ferrite metastable austenite shows two characteristic pop-ins which can be attributed to strain induced transformation from austenite to martensite (Fig. 7c). Especially the change in slope after the pop-ins is characteristic for the martensitic transformation. Furthermore, the phase transformation can be substantiated by an EBSD analysis in the plastic zone underneath the indents, showing the formation of martensite lamellae in metastable austenite (Fig. 7b).

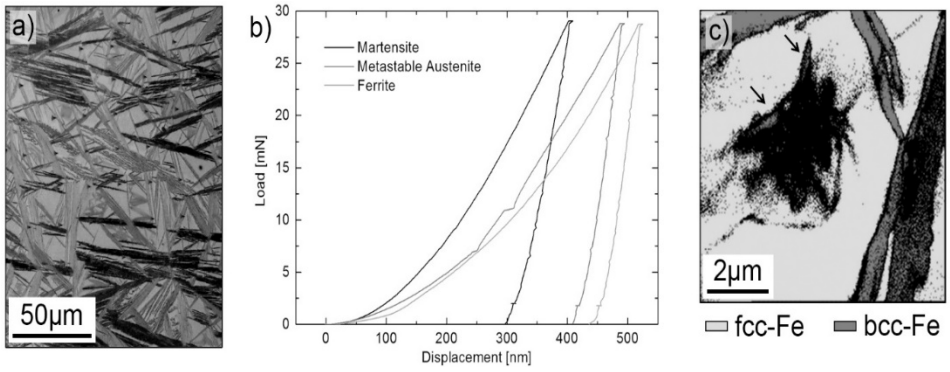

Fig. 7: a) Typical microstructure of Austempered Ductile Iron, b) load displacement curves for different phases in ADI probed with the NanoFlip and c) EBSD phase analysis in the plastic zone of an ident in metastable austenite showing the formation of strain induced martensite (indicated by arrows).

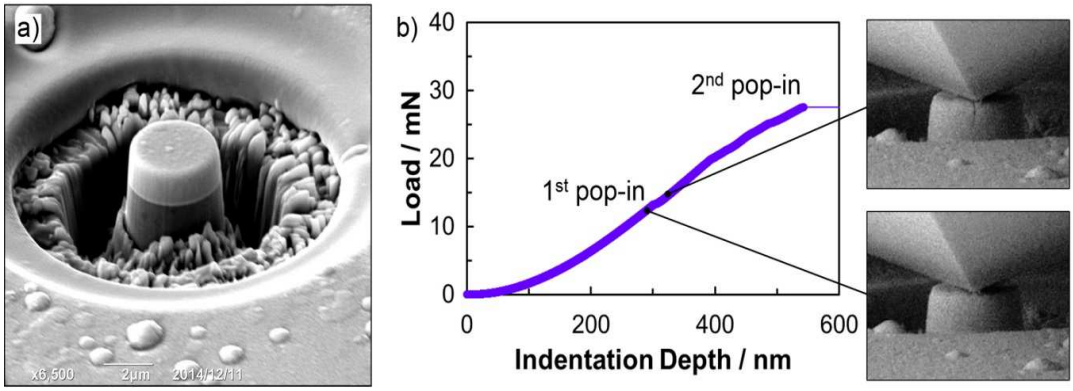

Fig. 8:
a) Side view of a FIB prepared pillar and b) load displacement curve of in-situ pillar splitting experiment with correspondent SEM images before and just after the first pop-in.

SEM video files captured during in-situ testing synchronized with the mechanical test data enable time resolved correlation of specific test events like inelastic deformation or fracture of the sample under investigation with the correspondent mechanical data. Fig. X gives an example of analyzing the cracking of a 1.5 µm thick a-C:H:W coating deposited on steel substrate. A pillar with a diameter of about 3.5 µm (Fig. 7a) was prepared by FIB using a JEOL JIB 4600F. Two pop-ins, a small and a large one, were observed in the force displacement curve (Fig. 7b). Both could be correlated to specific failure mechanisms of the coating by means of in-situ observation. The first small pop-in could be attributed to cracking of the coating and the second to catastrophic failure of the pillar probably caused by delamination at the interface. After the test the sample stage was rotated by 90° and the sample was aligned in line with the SEM for high resolution imaging and detailed failure analysis. The pillar was hit in its center, giving evidence for the high positioning accuracy, and split in three equal parts, which seem to be delaminated at the interface between the coating and the steel substrate (Fig. 8a).

For the evaluation of the experimental data Finite Element Analysis (FEA) is needed. A qualitative good agreement between experiment and simulation was observed. Fig. 8b) shows the crack propagation (rough textured surface) before and after first pop-in together with the correspondent force displacement curves extracted from FEA. The force displacement curve of FEA also shows two pop-ins. Here the opportunity to directly watch the experiment synchronized with the mechanical test data is of particular importance for the analysis of the experiment and a fundamental understanding of the relevant cracking mechanisms.

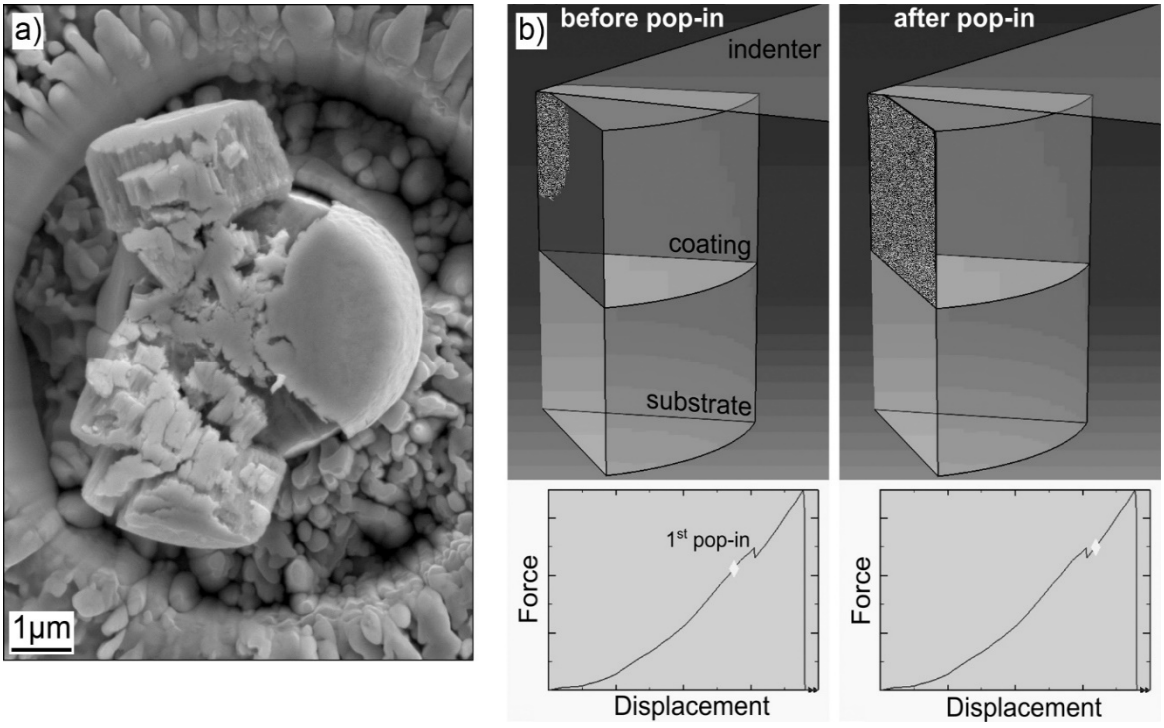

Fig. 8: (a) Top view of the pillar directly captured after testing and (b) visualization of crack propagation before and after first pop-in together with the correspondent force displacement curves extracted from FEA. Here a drop in force instead of displacement is visible since the simulations were performed under displacement control.